THE JOURNAL OF BIOLOGICAL CHEMISTRY VOL. 283, NO. 40, pp. 26902–26910, October 3, 2008

Dictyostelium Myosin-5b Is a Conditional Processive Motor*[S]

Received for publication, April 17, 2008, and in revised form, July 15, 2008 Published, JBC Papers in Press, July 23, 2008, DOI 10.1074/jbc.M802957200

Manuel H. Taft, Falk K. Hartmann, Agrani Rump, Heiko Keller, Igor Chizhov, Dietmar J. Manstein, and Georgios Tsiavaliaris[1]

From the Institute for Biophysical Chemistry, OE 4350, Hannover Medical School, Feodor-Lynen-Str. 5, D-30625 Hannover, Germany

***Dictyostelium* myosin-5b is the gene product of *myoJ* and one of two closely related myosin-5 isoenzymes produced in *Dictyostelium discoideum*. Here we report a detailed investigation of the kinetic and functional properties of the protein. In standard assay buffer conditions, *Dictyostelium* myosin-5b displays high actin affinity in the presence of ADP, fast ATP hydrolysis, and a high steady-state ATPase activity in the presence of actin that is rate limited by ADP release. These properties are typical for a processive motor that can move over long distances along actin filaments without dissociating. Our results show that a physiological decrease in the concentration of free Mg^{2+}-ions leads to an increased rate of ADP release and shortening of the fraction of time the motor spends in the strong actin binding states. Consistently, the ability of the motor to efficiently translocate actin filaments at very low surface densities decreases with decreasing concentrations of free Mg^{2+}-ions. In addition, we provide evidence that the observed changes in *Dd* myosin-5b motor activity are of physiological relevance and propose a mechanism by which this molecular motor can switch between processive and non-processive movement.**

Class 5 myosins are dimeric actin-based motors that are involved in various forms of intracellular trafficking (1). Dependent on the isoform and cell type, class 5 myosins have been implicated in the movement of membranes and organelles (2–4), the transport of synaptic and secretory vesicles (5, 6), and the active delivery of receptors and mRNA-protein complexes to their place of action (7, 8). The unique modular structure of class 5 myosins is essential for these specialized transport functions (9, 10). Each heavy chain of a dimeric myosin-5 molecule consists of a motor domain that binds actin and hydrolyzes ATP (11), followed by a long neck region to which up to six light chains can bind (12, 13). Parts of the adjacent tail region form a coiled-coil and the C terminus consists of a globular domain that mediates the binding to cargo and regulates activity of the motor (14, 15).

Despite the high sequence similarity between myosin-5 isoforms, the individual members display differences in their mechanoenzymatic properties, which characterize them either as processive or non-processive motors. Processive myosins, like vertebrate myosin-5a, are capable of taking successive steps along actin as single molecules before detaching (16). The overall movement has been described as a coordinated stepping process of both heads in a hand-over-hand mechanism that is driven by intramolecular strain (17, 18). In contrast, non-processive myosins bind to the actin filament perform just one step and then dissociate rapidly. A notable difference between processive and non-processive myosins is displayed in the duty ratio, *i.e.* the fraction of the total ATPase cycle time a motor spends in the strong actin binding states. Processive myosins have a high duty ratio (>0.5), whereas non-processive myosins display a low duty ratio that is generally far below 0.5. Characteristic kinetic parameters contributing to a high duty ratio thus minimizing early detachment from actin include (i) a fast ATP hydrolysis rate, (ii) a high affinity for actin in the weak binding states, (iii) a high ADP affinity in the actin-bound states, (iv) a rate-limiting ADP dissociation rate, (v) an increased P_i release rate, and (vi) a weak coupling between nucleotide and actin binding sites.

The relevance of a high duty ratio for processive movement has been shown by comparison of the kinetic properties of class 5 myosins from different subclasses and organisms. Accordingly, vertebrate myosin-5a is a high duty ratio motor that moves processively along actin filaments (19, 20). Recently, a kinetic study of human myosin-5b revealed that this myosin is also characterized by a high duty ratio; however, direct observation of the predicted processivity has not been reported (21).

Not all class 5 myosins are high duty ratio motors. *Homo sapiens* myosin-5c (22, 23), *Drosophila melanogaster* myosin-5 (24), and *Saccharomyces cerevisiae* myo2p and myo4p (25, 26) display properties that are not compatible with those of a processive motor. It is assumed that these myosins need to function as ensembles for the efficient intracellular translocation of cargo. So far, there is limited information about the kinetic, structural, and mechanoenzymatic properties of class 5 myosins that belong to subclasses other than subclass 5a. Thus, it is difficult to define in detail the parameters and molecular mechanisms that distinguish processive class 5 myosins from non-processive ones. The members of the respective groups are assumed to use different ways to couple conformational changes at the nucleotide binding regions to changes that occur at the actin binding sites during the ATPase cycle.

This study provides a detailed kinetic and functional characterization of *Dictyostelium discoideum* myosin-5b (*Dd*

* The work was supported by Deutsche Forschungsgemeinschaft Grants TS 169/3-1 (to G. T.) and MA 1081/11 (to D. J. M.). The costs of publication of this article were defrayed in part by the payment of page charges. This article must therefore be hereby marked "*advertisement*" in accordance with 18 U.S.C. Section 1734 solely to indicate this fact.

[S] The on-line version of this article (available at http://www.jbc.org) contains supplemental Movies 1 and 2.

[1] To whom correspondence should be addressed: Institut für Biophysikalische Chemie, OE 4350, Medizinische Hochschule Hannover, Carl-Neuberg-Straße 1, D-30625 Hannover, Germany. Tel.: 49-511-532-8591; Fax: 49-511-532-5966; E-mail: gtsiaval@bpc.mh-hannover.de.

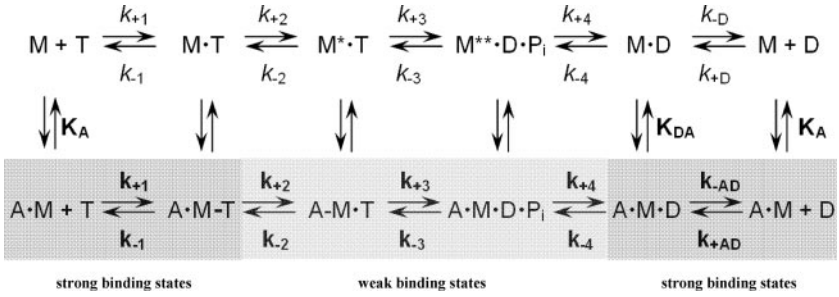

Scheme 1. **Kinetic reaction scheme of the actomyosin ATPase cycle.** *A* refers to actin, *M* to myosin, *T* to ATP, and *D* refers to ADP. Rate constants are referred to as k_{+n} and k_{-n} is assigned to the corresponding forward and reverse reactions. An additional notation is used that distinguishes between the constants in the absence and presence of actin by italic type (k_{-1}, K_1) and bold ($\mathbf{k_{-1}}$, $\mathbf{K_1}$), respectively; subscript *A* refers to actin ($\mathbf{K_A}$) and subscripts D (K_D) refers to ADP.

myosin-5b),[2] a heavy chain dimer forming class 5 myosin, which previously has been referred to as MyoJ (27, 28). We compare the results obtained for *Dd* myosin-5b with those previously reported for processive and non-processive members of the myosin-5 family (19, 21–24). Our investigations reveal that under standard assay conditions the kinetic properties of *Dd* myosin-5b are similar to those of other processive myosins: ADP-release limiting the actomyosin ATPase cycle, a low degree of coupling between the nucleotide and actin binding sites, and a high duty ratio. We show that changes in the concentrations of free Mg^{2+}-ions that lie in the physiological range modulate the ADP release kinetics of the motor and affect the duty ratio, which is a critical determinant for processivity. Our results show that this particular mechanism enables native *Dd* myosin-5b to switch between processive and non-processive motor activity in the context of the contractile vacuole.

EXPERIMENTAL PROCEDURES

Reagents—Standard chemicals, TRITC-phalloidin, and anti-His antibody were purchased from Sigma; restriction enzymes, polymerases, and DNA-modifying enzymes were purchased from MBI-Fermentas and Roche Applied Sciences.

Plasmid Construction—The oligonucleotides 5′-C GGA TCC ACC ACA TCA ACA ATT-3′ and 5′-GT CTC GAG CAC TAC GAT CCA-3′ were used to isolate a PCR fragment from *Dictyostelium* AX2 genomic DNA that encodes the 829 amino acids of the motor domain of *Dictyostelium* myosin-5b (28). The product was cloned into the expression vector pDXA-3H between restriction sites BamHI and XhoI (pDXA-J829) (29). The introduction of the extra XhoI site created mutation T829R in the protein. A motor domain construct fused to two *D. discoideum* α-actinin repeats (J829-2R) was obtained as the XhoI/SphI fragment from pM790-2R-eYFP (30) and inserted in the XhoI/SphI-digested pDXA-J829 motor domain expression plasmid. To produce full-length *Dd* myosin-5b fused to EYFP, base pairs 2692–6947 starting from the open reading frame of the *Dd* myosin-5b gene were amplified by PCR from genomic DNA and inserted into the pDXA-J829 expression vector using XhoI as a unique restriction site. This produced the plasmid pDXA-*Dd* myosin-5b encoding the full-length protein. It was digested with BamHI and SphI and the gene fragment was cloned into the vector pDXA-EYFP-MCS for the N-terminal fusion with EYFP (29). All plasmids were confirmed by sequencing.

Protein Production and Purification—Plasmids for the high level production of the *Dd* myosin motor domain constructs were transformed into AX3-Orf$^+$ cells by electroporation as described earlier (31, 32). The full-length EYFP-*Dd* myosin-5b plasmid was transformed for cell biological investigations in AX2 cells. Transformants were grown at 21 °C in HL-5c medium and selected in the presence of 10 μg/ml G418 and 100 units/ml penicillin/streptomycin. Screening for the production of the recombinant myosins and protein purification was performed as described (33). Rabbit skeletal muscle actin was purified as described by Lehrer and Kerwar (34) and pyrene-labeled actin was prepared as described by Criddle *et al.* (35).

Kinetic Measurements—ATPase activities were measured at 25 °C with the NADH-coupled assay as described previously (36). Values for k_{cat} and K_{app} were calculated from fitting the data to the Michaelis-Menten equation. Transient kinetic experiments were performed at 20 °C with either a Hi-tech Scientific SF-61 DX single mixing stopped-flow system or an Applied Photophysics PiStar 180 Instrument in MOPS buffer (25 mM MOPS, 100 mM KCl, 1 mM dithiothreitol, pH 7.0) supplemented with varying concentrations of $MgCl_2$ using procedures and kinetic models described previously (37). Free Mg^{2+}-ion concentrations were calculated using Maxchelator software as described (38). Kinetic parameters of nucleotide and actin interactions were analyzed in terms of the model shown in Scheme 1.

Direct Functional Assays—Actin-sliding motility was measured as described previously (30). The movement of more than 200 TRITC-phalloidin-labeled actin filaments was recorded for each individual concentration of free Mg^{2+}-ions. Automated actin filament tracking was performed with the program DiaTrack 3.01 (Semasopht, Switzerland) and data analysis was performed with Origin 7.0 (Originlab, USA).

Landing assays were performed as described by Rock *et al.* (39) with the following modifications: *Dd* myosin-5b molecules were immobilized on nitrocellulose-coated coverslips via anti-penta-His antibodies (concentration range 0.5 to 41 μg/ml) to obtain surface densities between 50 and 4000 myosin molecules/μm^2. The assay was started by the addition of TRITC-phalloidin-labeled actin (100 nM) to the motility buffer (described above) containing 1.5 mM Mg^{2+}-ATP and varying concentrations of free Mg^{2+}-ions. The landing events were recorded with an objective type TIRF microscope equipped with a 532 nm diode laser (150 milliwatts). An inverted micro-

[2] The abbreviations used are: *Dd* myosin-5b, *Dictyostelium discoideum* myosin-5b; *Dm* myosin-5, *Drosophila melanogaster* myosin-5; TRITC, tetramethylrhodamine isothiocyanate; MOPS, 3-(*N*-morpholino)propanesulfonic acid; KMG-104AM, 1-(6-acetoxy-2,7-difluoro-3-oxo-3*H*-xanthen-9-yl)-4-oxo-4*H*-quinolizine-3-carboxylic acid acetoxymethyl ester; EYFP, enhanced yellow fluorescent protein.

TABLE 1
Steady-state ATPase activities

Myosin	Basal ATPase	Michaelis-Menten parameters			Activation[c]
		k_{cat}[a]	K_{app}[a]	k_{cat}/K_{app}[b]	
	s^{-1}	s^{-1}	μM	μM^{-1}	s^{-1}
Dd myosin-5b[d]	0.069 ± 0.01	12.4 ± 0.5	21 ± 2	0.59 ± 0.12	179 ± 12
Hs myosin-5b[e]	0.09	9.7	8.5	1.14	107
Gg myosin-5a[f]	0.03	15	1.4	11	500
Hs myosin-5c[g]	0.1/0.05	6.5/1.8	62/42.5	0.1/0.042	64/35
Dm myosin-5[h]	0.1	12.5	9.9	1.26	125

[a] Values for k_{cat} and K_{app} were calculated from fitting the data to the Michaelis-Menten equation.
[b] The apparent second order rate constant for actin binding (k_{cat}/K_{app}) was obtained from the calculated ratio of both values.
[c] ATPase activation = (k_{cat} − basal ATPase)/basal ATPase.
[d] Experimental conditions: 25 mM HEPES, 25 mM KCl, 5 mM $MgCl_2$, 1 mM dithiothreitol, 1 mM ATP, pH 7.3.
[e] Watanabe *et al.* (21).
[f] De La Cruz *et al.* (19).
[g] Watanabe *et al.* (22) and Takagi *et al.* (23), respectively.
[h] Tóth *et al.* (24).

scope was used (Olympus IX81) fitted with a 60 × 1.49 NA oil immersion lens (ApoN, Olympus). The landing rate was measured by counting the number of actin filaments that landed and moved ≥0.5 μm in an observation area of ~12,000 μm^2.

Cell Imaging—The cellular localization of *Dd* myosin-5b was assayed by confocal microscopy with an inverted Leica TCS SP2 AOBS microscope. Cells transfected with EYFP-*Dd* myosin-5b were seeded on glass bottom Petri dishes (coverslip thickness: 160–180 μm), washed twice with Bonner's salts solution (10 mM NaCl, 10 mM KCl, and 3 mM $CaCl_2$), and kept in this medium during image acquisition. Images were recorded at 21 °C at one frame per 10-s interval with a 63 × 1.4 NA immersion oil objective. The excitation wavelength was 514 nm; fluorescence emission was detected from 528 to 600 nm. Image processing was done with the Leica Confocal Software.

Experiments with the fluorescent dye KMG-104AM were performed according to Ref. 40 using the TIRF setup described above. Cells were incubated in 10-ml flasks with shaking at 180 rpm in the presence of 40 μM KMG-104AM. KMG-104AM was dissolved in 50 mM HEPES, pH 7.3. After 2 h cells were seeded on Petri dishes and immediately before imaging the solution containing KMG-104AM was replaced by 50 mM HEPES, pH 7.3, containing 10 mM $MgCl_2$.

RESULTS

All kinetic experiments were performed with a single-headed *Dd* myosin-5b construct (J829) comprising 829 amino acids of the motor domain. Nucleotide and actin interactions were analyzed according to Scheme 1.

Steady-state ATPase Activity of Dd Myosin-5b—The steady-state ATPase activity of *Dd* myosin-5b was measured in the absence and presence of actin in the range from 0 to 60 μM actin. *Dd* myosin-5b displays a basal ATPase rate (k_{basal}) of 0.069 s^{-1}. The maximum actin-activated ATPase activity (k_{cat}) is 12.4 s^{-1} and comparable with the steady-state ATPase rates reported for other class 5 myosins. Half-maximal activation of the ATPase (K_{app}) is reached at 21 μM F-actin and the apparent second-order rate constant for actin binding (k_{cat}/K_{app}) is 0.59. The obtained steady-state parameters are summarized in Table 1, together with published values of human myosin-5b (*H. sapiens* myosin-5b), chicken myosin-5a (*Gallus gallus* myosin-5a), human myosin-5c (*H. sapiens* myosin-5c), and *Drosophila* myosin-5 (*Dm* myosin-5).

ATP Binding to Dd Myosin-5b and ATP-induced Dissociation of Acto·Dd Myosin-5b—ATP binding to the *Dd* myosin-5b motor domain was monitored from the increase in intrinsic protein fluorescence following the addition of ATP. Fluorescence transients were best fit to single exponentials at all ATP concentrations examined. In the range from 5 to 25 μM ATP, the observed rate constants were linearly dependent upon ATP concentration. The apparent second-order rate constant obtained from the slope corresponds to $K_1k_{+2} = 0.47\ \mu M^{-1}\ s^{-1}$. At higher ATP concentrations the observed rate constants k_{obs} followed a hyperbolic dependence (Fig. 1*A*, *filled circles*). At saturating ATP concentrations, k_{max} defines the maximum rate of the conformational change that corresponds to the rate of ATP hydrolysis in the absence of actin ($k_{+3} + k_{-3}$). In the case of *Dd* myosin-5b this rate is >300 s^{-1} (Table 2).

ATP binding to acto·*Dd* myosin-5b was followed by observing the exponential increase in fluorescence of pyrene-actin as the actomyosin complex dissociates following the addition of excess ATP. The mechanism of ATP-induced fluorescence enhancement was modeled according to Scheme 2, which describes a two-step mechanism for ATP binding to actomyosin.

$$A \cdot M + ATP \underset{}{\overset{K_1}{\rightleftharpoons}} A \cdot M \cdot ATP \xrightarrow{k_{+2}} A + M \cdot ATP$$

SCHEME 2

At lower ATP concentrations the observed rate constants increased linearly up to 50 μM ATP giving a second-order rate binding constant $\mathbf{K_1k_{+2}}$ of 0.19 ± 0.01 $\mu M^{-1}\ s^{-1}$ (Fig. 1*A*, *filled squares*). At higher ATP concentrations the increase of the observed rate constants (k_{obs}) was best described by a hyperbola, approaching a maximum value $\mathbf{k_{+2}}$ of ~75 s^{-1} and an apparent equilibrium constant for ATP binding of $\mathbf{K_1} > 400\ \mu M$.

ADP Binding to Dd Myosin-5b in the Presence and Absence of Actin—Because binding of ADP to the motor domain of *Dd* myosin-5b did not result in a change of the fluorescence signal, neither in the absence nor presence of F-actin measurements were performed using the fluorescent analogue mantADP. Binding of mantADP was determined by monitoring the increase in mant-fluorescence upon the addition of increasing concentrations of the fluorescent analogue to the *Dd* myosin-5b motor domain construct. In the range from 1 to 30 μM mantADP, time courses of mantADP binding to *Dd* myosin-5b and acto·*Dd* myosin-5b followed single exponentials with rates that were linearly dependent on the concentration of nucleotide (Fig. 1*B*). The apparent second-order rate constants for ADP binding to *Dd* myosin-5b (k_{+D}) and acto·*Dd* myosin-5b ($\mathbf{k_{+AD}}$) were determined from the slopes of the straight lines fitted to the data. The ratio of $\mathbf{k_{+AD}} = 4.0\ \mu M^{-1}\ s^{-1}$ and $k_{+D} = 0.17\ \mu M^{-1}\ s^{-1}$ indicates that the rate of ADP binding is more than 20-fold increased in the presence of actin (Table 2).

Actin Binding Properties of Dd Myosin-5b—The rate of actin binding was measured by following the exponential decrease in pyrene fluorescence upon binding of excess pyrene-labeled

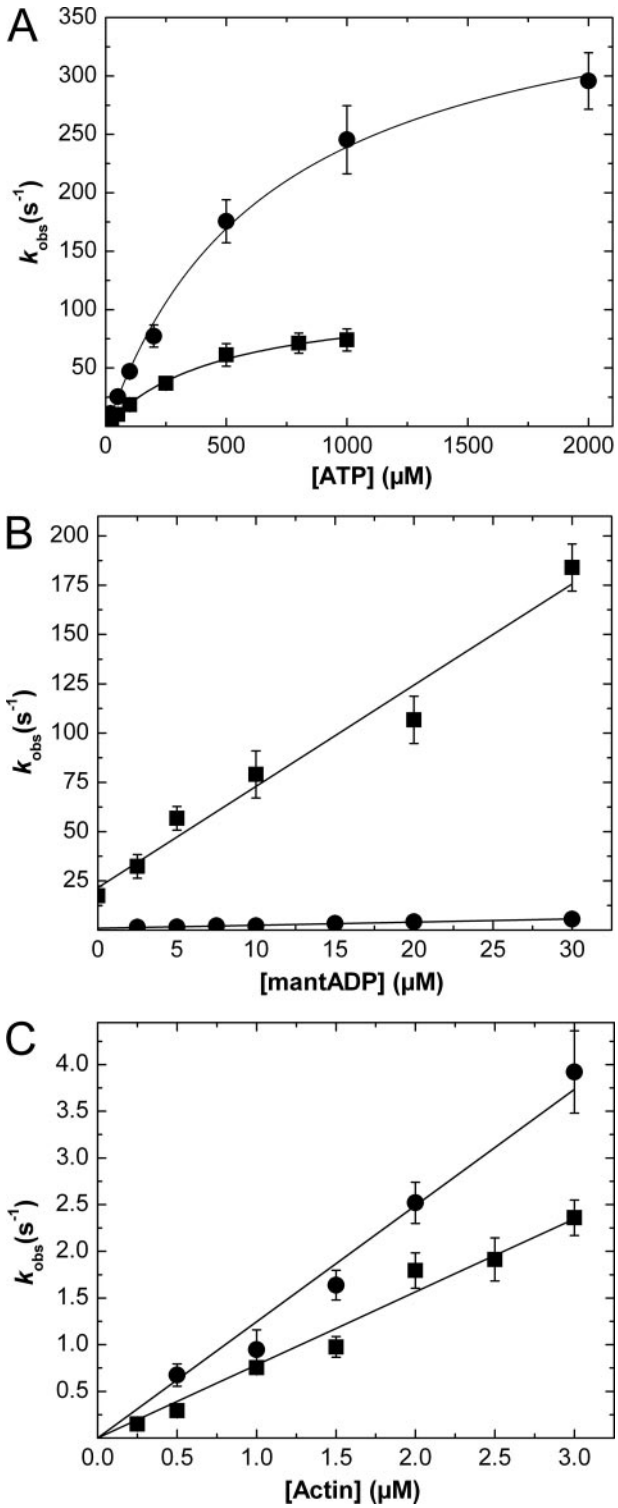

FIGURE 1. **Transient kinetic analysis of the interaction of nucleotides with *Dd* myosin-5b and acto·*Dd* myosin-5b.** *A*, ATP binding to *Dd* myosin-5b (●) and ATP-induced dissociation of acto·*Dd* myosin-5b (■). Hyperbolic dependence of the observed rate constant k_{obs} on ATP concentrations in the range of 0.005 to 1 mM. At low ATP concentrations k_{obs} were linearly dependent upon ATP concentration. The apparent second-order rate constant for ATP binding to myosin and actomyosin were determined from the slope of the straight lines. The rate constants for the ATP hydrolysis reaction $k_{+3} + k_{-3}$ in the absence of actin and the isomerization step k_{+2}, respectively, are given by the plateau values. *B*, mantADP binding to *Dd* myosin-5b (●) and acto·*Dd* myosin-5b (■) upon mixing 1 μM *Dd* myosin-5b and 1 μM acto·*Dd*Myosin-5b, respectively, with increasing mantADP concentrations (0–30 μM). The observed rate constants were determined by fitting the time courses of the fluorescence change to single exponentials and plotted against the mantADP concentration. *C*, actin binding to *Dd* myosin-5b in the absence (●) and presence of ADP (■). The observed rate constants were plotted against the pyrene-actin concentration and second-order rate constants were obtained from linear fits to the data. All rate and equilibrium constants are summarized in Table 2.

actin to the *Dd* myosin-5b motor domain. The observed rate constants were linearly dependent upon F-actin concentration over the range studied (Fig. 1*C*, *filled circles*). The data were modeled as simple bimolecular reactions. The apparent second-order rate constant of pyrene-actin binding ($\mathbf{k_{+A}}$) was obtained from the slope of the plot giving a value for $\mathbf{k_{+A}}$ of 1.17 μM^{-1} s^{-1}. The presence of 1 mM ADP did not significantly affect the second-order rate binding constant ($\mathbf{k_{+DA}}$) of F-actin to *Dd* myosin-5b (Fig. 1*C*, *filled squares*).

Pyrene-actin dissociation from *Dd* myosin-5b was measured by competition with F-actin after mixing an equilibrated mixture of pyrene-acto·*Dd* myosin-5b with a 40-fold excess of unlabeled F-actin. In the absence and presence of ADP, the observed processes could be fit to single exponentials were k_{obs} corresponds directly to $\mathbf{k_{-A}}$ and $\mathbf{k_{-DA}}$, respectively. The rates of actin displacement in the absence and presence of 1 mM ADP ($\mathbf{k_{-A}} = 0.023 \pm 0.001$ μM^{-1} s^{-1} and $\boldsymbol{k_{-DA}} = 0.03 \pm 0.001$ s^{-1}) are very similar and indicate that the tight association of F-actin to *Dd* myosin-5b is not affected by the presence of excess amounts of ADP. Furthermore, the apparent acto·*Dd* myosin-5b affinities ($\mathbf{K_A}$ and $\mathbf{K_{DA}}$) were determined from the ratio of the rate constants for actin binding and dissociation. The parameters are summarized in Table 2.

ADP Dissociation from Dd Myosin-5b and Acto·Dd Myosin-5b—The rate of ADP dissociation was determined by monitoring the decrease in fluorescence upon displacement of *mantADP* from the *myosin-mantADP* and *actomyosin-mantADP* complex by the addition of excess *ADP.* The observed processes could be fitted to single exponentials where k_{obs} corresponds directly to the ADP dissociation rates k_{-D} in the absence and $\mathbf{k_{-AD}}$ in the presence of actin (Scheme 1). MantADP dissociation from *Dd* myosin-5b was ~25-fold increased by actin from $k_{-D} = 0.92$ s^{-1} to $\mathbf{k_{-AD}} = 21.6$ s^{-1} (Table 2).

ADP Affinity of Dd Myosin-5b in the Absence and Presence of Actin—The affinity of ADP for *Dd* myosin-5b was determined by monitoring the reduction in the rate of pyrene-actin binding to the myosin motor domain as a function of ADP concentration. The decrease in pyrene fluorescence followed single exponentials at all ADP concentrations examined. The k_{obs} values plotted against the ADP concentration are shown in Fig. 2*A*. High ADP concentrations decreased the observed rate of pyrene-actin binding ~2-fold. Fitting the data to a hyperbola gives an affinity constant of ADP for *Dd* myosin-5b (K_D) of 5.5 μM. This value is consistent with the calculated affinity constant $K_D = 5.4$ μM obtained from k_{-D}/k_{+D}.

The affinity of ADP for the actomyosin complex ($\mathbf{K_{AD}}$) was determined from the inhibition of the ATP-induced dissociation of acto·*Dd* myosin-5b by ADP. The observed rate of actin dissociation from *Dd* myosin-5b was reduced up to 8-fold when excess ATP was added to the actomyosin complex in the presence of varying concentrations of ADP. The dissociation reactions were monophasic and best described by single exponen-

TABLE 2
Summary of the rate and equilibrium constants of the actomyosin interactions in the presence and absence of nucleotides

	Constant	*Dd* myosin-5b[a]	*Hs* myosin-5b[b]	*Gg* myosin-5a[c]	*Hs* myosin-5c[d,e]	*Dm* myosin-5[f]
Nucleotide binding to myosin						
ATP	K_1k_{+2} (μM^{-1} s^{-1})	0.47 ± 0.02	0.31	1.6	2.5	1.31
	$k_{+3} + k_{-3}$ (s^{-1})	>300		≥750	59/90	68
ADP	K_D (μM)	5.5 ± 0.9				
mantADP	K_{+D} (μM^{-1} s^{-1})	0.17 ± 0.01		3.7	2.9	2.2
	k_{-D} (s^{-1})	0.92 ± 0.1		1.9	3.6	38.3
	K_D (μM)	5.4 ± 0.9		0.51	1.24	17
Nucleotide binding to actomyosin						
ATP	$\mathbf{K_1k_{+2}}$ (μM^{-1} s^{-1})	0.19 ± 0.01	0.31	0.9	1.8/0.82	0.36
	$\mathbf{k_{+2}}$ (s^{-1})	>75		870	>300/287	>180
ADP	$\mathbf{K_{AD}}$ (μM)	8 ± 1.3			0.25	
	$\mathbf{k_{-AD}}$ (s^{-1})	17.4 ± 1.7	11.7	16	15.8	
mantADP	$\mathbf{k_{+AD}}$ ($\mu M^{-1}s^{-1}$)	4.0 ± 0.7		12.6	6	4.7
	$\mathbf{k_{-AD}}$ (s^{-1})	21.6 ± 6	11.1	12	17.7/15.6	150
	$\mathbf{K_{AD}}$ (μM)[g]	5.4 ± 2		0.93	2.1	32
	$\mathbf{K_{AD}}/K_D$	1 ± 0.41		1.8	1.7	1.9
Actin binding to myosin						
	$\mathbf{K_{+A}}$ ($\mu M^{-1}s^{-1}$)	1.17 ± 0.08		73	1.11/0.66	2.5
	$\mathbf{k_{-A}}$ (s^{-1})	0.023 ± 0.001		0.00036	0.011/0.019	0.04
	$\mathbf{K_A}$ (nM)	20 ± 2		0.005	9.9/29	16
Actin binding to myosin in the presence of ADP						
	$\mathbf{k_{+DA}}$ ($\mu M^{-1}s^{-1}$)	0.78 ± 0.06		4.2	0.88/1.17	2.3
	$\mathbf{k_{-DA}}$ (s^{-1})	0.03 ± 0.001		0.032	0.0099/0.051	0.43
	$\mathbf{K_{DA}}$ (nM)	38.5 ± 5		7.6	11.3/44	190
Duty ratio[h]		0.74 ± 0.05 0.23 ± 0.05[i]	0.79	0.95	0.39/0.12	0.12

[a] Experimental conditions: 25 mM MOPS, 100 mM KCl, 5 mM $MgCl_2$, 1 mM dithiothreitol, pH 7.0.
[b] Watanabe *et al.* (21).
[c] De La Cruz *et al.* (19).
[d] Watanabe *et al.* (22).
[e] Takagi *et al.* (23).
[f] Tóth *et al.* (24).
[g] K_{AD} (μM) = (k_{-AD}/ k_{+AD}).
[h] Calculated values according to Equation 2 at 5 mM free Mg^{2+}-ion.
[i] Calculated values according to Equation 2 at 0.2 mM free Mg^{2+}-ion concentrations.

tials. The determined rate constants were plotted against the ADP concentration and the data were fitted to a hyperbola (Fig. 2*B*) yielding a dissociation equilibrium constant ($\mathbf{K_{AD}}$) of 8 μM. At high ADP concentrations the dissociation rate constant of the acto·*Dd* myosin-5b complex by 2 mM ATP decreased to 17.4 ± 1.9 s^{-1}. Because ADP release from the A·M·D complex limits the rate of the ATP-induced dissociation, the rate of 17.4 s^{-1} corresponds directly to the ADP dissociation rate from acto·myosin (k_{-AD}). F-actin has minimal effects on the affinity of ADP to *Dd* myosin-5b, although both binding and dissociation rates are affected by the presence of actin. In addition the association constant of actin for *Dd* myosin-5b in the presence of ADP ($\mathbf{K_{DA}}$) was calculated as follows: $\mathbf{K_{DA}} = \mathbf{K_{AD}}/K_D \times \mathbf{K_A}$. The resulting affinity for actin in the presence of ADP ($\mathbf{K_{DA}}$) is 56 nM and comparable with the value calculated from of $\mathbf{K_{DA}} = \mathbf{k_{-DA}}/\mathbf{k_{+DA}}$ = 38.5 nM (Table 2).

Effect of Free Mg^{2+} Ions on ADP Binding Kinetics to Acto·Dd Myosin-5b—We examined the kinetics of ADP binding to acto·*Dd* myosin-5b by mixing nucleotide-free acto·*Dd* myosin-5b with increasing concentrations of mantADP in the presence of 0.2, 1, 3, and 5 mM free Mg^{2+}-ions. The resulting fluorescence increase followed single exponential functions at all conditions. The observed rate constants increased linearly with increasing ADP concentration (Fig. 3*A*). The second-order rate constant ($\mathbf{k_{+AD}}$) determined from the slope of the linear fit to the data ranged from 4.0 ± 0.7 to 6.7 ± 0.4 μM^{-1} s^{-1}. In contrast, the ADP dissociation rates ($\mathbf{k_{-AD}}$) as obtained from the *y* intercepts of the straight lines decreased with increasing concentrations of free Mg^{2+}-ions. The Mg^{2+}-ion dependence of the ADP dissociation from the actomyosin complex was further confirmed by directly measuring the rate of ADP dissociation from acto·*Dd* myosin-5b using the fluorescent analogue mantADP. In the presence of 0.2, 1, 3, 4.3, and 5 mM free Mg^{2+}-ions, the time courses for the observed fluorescence change after mixing acto·*Dd* myosin-5b-mantADP with 1 mM ADP follow single exponentials (Fig. 3*B*, *inset*). The apparent rate constant for mantADP release ($\mathbf{k_{-AD}}$) dropped from 187 ± 25 s^{-1} at 0.2 mM free Mg^{2+} to 17.4 ± 1.9 s^{-1} at 5 mM Mg^{2+}. The observed inverse hyperbolic dependence of the rate of mantADP on the free Mg^{2+} concentration is described by Equation 1,

$$\mathbf{k_{-AD}} = \frac{(k_{min} \cdot [Mg^{2+}]/K_i) + k_{max}}{([Mg^{2+}]/K_i) + 1} \quad \text{(Eq. 1)}$$

where $\mathbf{k_{-AD}}$ is the observed rate constant, k_{max} is the rate constant at 0 μM free Mg^{2+}-ions, k_{min} the rate constant at saturating free Mg^{2+}-ion concentrations, and K_i is the apparent inhibition constant for free Mg^{2+}-ions, which is 0.44 ± 0.1 mM (Fig. 3*B*).

Influence of Free Mg^{2+} Ions on the Motile Activity of Dd Myosin-5b—The motor activity of *Dd* myosin-5b was studied using the *in vitro* motility assay with a motor domain construct fused to an artificial lever-arm consisting of two α-actinin repeats. The ATP concentration was kept constant at 4 mM and the free Mg^{2+}-ion concentration was varied in the range from 0.01 to 20 mM. A maximum sliding velocity of 1.25 ± 0.12 μm/s

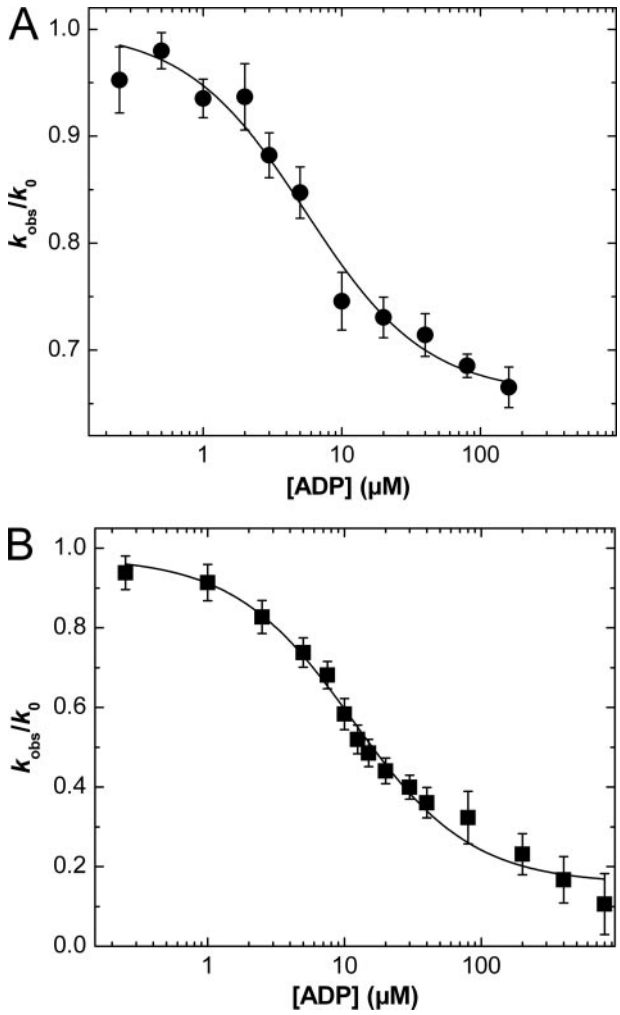

FIGURE 2. **ADP affinity of *Dd* myosin-5b in the presence and absence of actin.** *A*, inhibition of the rate of pyrene-actin binding to myosin head fragments (●). The ADP dissociation constant (K_D) of the *Dd* myosin-5b-ADP complexes were determined by fitting the plot k_{obs}/k_{+A} *versus* ADP concentrations with a hyperbola. *B*, affinity of ADP to acto·*Dd* myosin-5b (K_{AD}). K_{AD} was determined from the ADP inhibition of the ATP-induced dissociation of the actomyosin complex (■). Monophasic dissociation reactions were observed as the complex was dissociated with 1 mM ATP in the absence and presence of ADP. The observed rate constants were plotted against the ADP concentration, and the data were fitted with a hyperbola. All rate and equilibrium constants are summarized in Table 2.

was obtained at concentrations of free Mg^{2+}-ions between 10 and 50 μM. Increasing concentrations of free Mg^{2+}-ions that are within the physiological range (0.1 to 1 mM) reduce the motile activity of *Dd m*yosin-5b in a sigmoidal dependence up to 3-fold with an apparent inhibition constant for Mg^{2+}-ions (K_i) of 0.43 ± 0.05 mM (Fig. 3*C*) that is well consistent with the K_i obtained from Fig. 3*B* (0.44 ± 0.1 mM).

To assay the effect of Mg^{2+}-ions on the ability of *Dd* myosin-5b to bind and move actin filaments at very low surface densities, we performed landing assays at free Mg^{2+}-ion concentrations corresponding to 5 and 0.28 mM. The number of landing events decreased as the surface density of myosin molecules decreased. At 5 mM free Mg^{2+}-ions the landing rate was best fit to the equation: $L(\rho) = Z(1 - e^{-\rho/\rho 0})^n$, according to the model by Hancock and Howard (41) with $n = 1.25 \pm 0.2$ (Fig. 3*D*, *solid circles*) indicating that one *Dd* myosin-5b molecule is sufficient to bind and initiate movement. At 0.28 mM free Mg^{2+}-ions the number of landing events was drastically reduced and the data were best fit with $n = 18 \pm 2$ (Fig. 3*D*, *open circles*). At Mg^{2+}-ion concentrations <0.2 mM and myosin surface densities <3000 molecules/μm² no landing events could be observed.

Influence of Free Mg^{2+}-Ions on the Population of the Strong Actin Binding States and Duty Ratio of Dd Myosin-5b—The influence of free Mg^{2+}-ions on the population of strong actin binding states was assayed by two different experimental approaches. First, the dissociation reaction of the acto·myosin-5b complex by excess ATP was monitored at different free Mg^{2+} concentrations (Fig. 4*A*). A complex of 2 μM *Dd* myosin-5b and 15 μM pyrene-actin was dissociated by 50 μM ATP at 5 and 0.2 mM free Mg^{2+}-ion concentrations. The amplitudes were normalized and set in relation to the maximum change in fluorescence of *Dd* myosin-5b binding to pyrene-actin. An initial fast fluorescence decrease describing the dissociation of the complex is followed by a second, slower phase of re-association. At 5 mM free Mg^{2+} concentration the dissociation rate constant equals 4.2 s^{-1}, which is ~3 times slower than the rate observed at 0.2 mM free Mg^{2+}-ions (k_{obs} = 11.9 s^{-1}). As this dissociation reaction describes the conformational transition of myosin from high to low actin affinity, the slow dissociation rate at 5 mM free Mg^{2+}-ions indicates that *Dd* myosin-5b stays for a longer fraction of time strongly bound to actin than at 0.2 mM free Mg^{2+}-ions.

To further evaluate whether *Dd* myosin-5b is a high duty ratio motor at high Mg^{2+} concentrations and a low duty ratio motor at low Mg^{2+} concentrations, we performed sequential mixing experiments. A pre-equilibrated mixture of 4 μM myosin-5b and 20 μM pyrene-actin was rapidly mixed with 400 μM ATP, aged for 50 ms to allow ATP-binding, hydrolysis, and population of the weakly bound states (A·M·D·P_i), and then quenched with 2 mM ADP to prevent ATP binding to myosin (Fig. 4*B*). The final concentrations of pyrene-actin and myosin-5b after double mixing are 5 and 1 μM, respectively. The observed fluorescence quench is assumed as the transition from the high fluorescence weak binding states to the low fluorescence strong binding states (Scheme 1). At high concentrations of free Mg^{2+}-ions (5 mM, *upper trace*) the observed rate of the weak-to-strong transition is 2.0 ± 0.3 s^{-1} and the amplitude is 0.68. At 0.2 mM free Mg^{2+}-ions k_{obs} equals 1.5 ± 0.2 s^{-1} and the amplitude is decreased to 0.22 (Fig. 4*B*). Because both rate constants are similar to the steady-state ATPase rate (1.4 s^{-1}) that was obtained at 5 μM actin in the presence of 0.2 and 5 mM free Mg^{2+}-ions, we conclude that ATP turnover is limited by the weak-to-strong transition in both cases. Thus, free Mg^{2+}-ions have no influence on the actin activated steady-state ATPase rates. However, the differences in the amplitude of the pyrene-actin fluorescence at 0.2 and 5 mM free Mg^{2+}-ions indicate that 68 and 22% of the *Dd* myosin-5b molecules, respectively, are strongly bound to actin. These values provide direct estimates for the duty ratio (19).

Free Mg^{2+}-Ion Distribution in Dictyostelium Cells—To further elucidate the physiological relevance of the observed functional changes upon variation of the free Mg^{2+}-ion concentra-

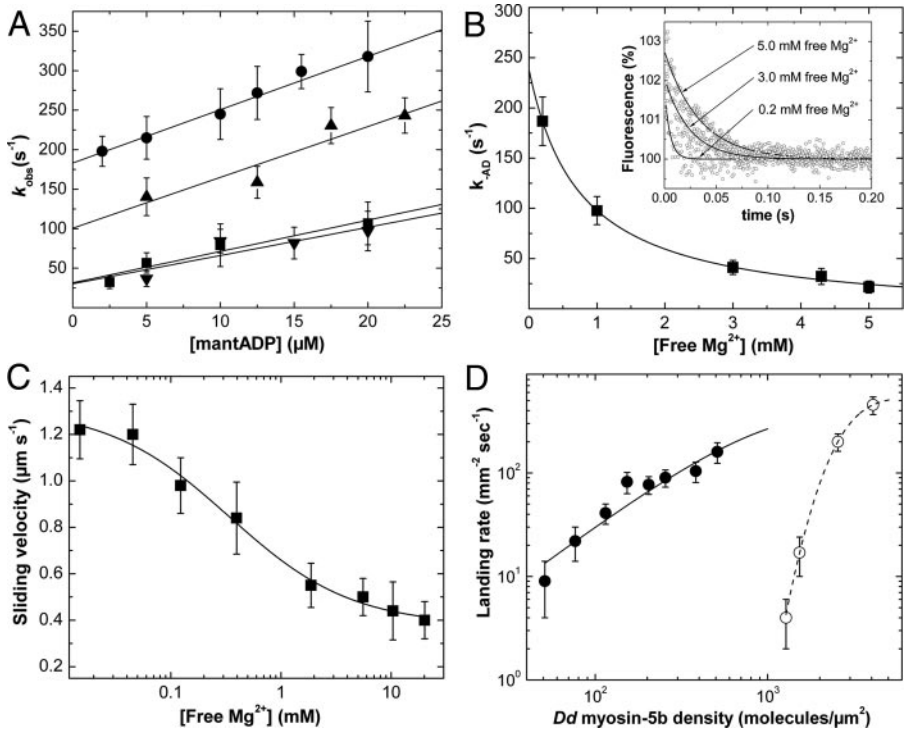

FIGURE 3. **Mg^{2+} dependence of ADP binding kinetics and motor activity.** *A*, effect of free Mg^{2+}-ions on mantADP binding to acto·*Dd* myosin-5b at 0.2 mM (●), 1 mM (▲), 3 mM (▼), and 5 mM (■) concentrations of free Mg^{2+}-ions. The slope of each plot defines an apparent second-order rate constant (k_{+AD}) for ADP binding to myosin and the *y* intercept defines a dissociation rate constant (k_{-AD}). *B*, Mg^{2+} dependence of mantADP dissociation from acto·*Dd* myosin-5b. The displacement of mantADP from the ternary mantADP·acto·*Dd* myosin-5b complex by excess unlabeled ADP at concentrations of free Mg^{2+}-ions from 0.2 to 5 mM was monitored from the resulting decrease of mant-fluorescence (*inset*). The data traces represent the averages of at least eight individual transients. The transients follow single exponentials and the observed dissociation rate constants (k_{-AD}) decrease in an inverse hyperbolical manner with increasing free Mg^{2+} concentrations. Excess free Mg^{2+} concentrations lead to a more than 10-fold decrease in the mantADP dissociation rate constant. *C*, dependence of *Dd* myosin-5b motor activity on free Mg^{2+}-ions. Uncertainties represent mean ± S.D. of at least three individual experiments. *D*, landing rate as a function of *Dd* myosin-5b surface density in the presence of 5 mM (*filled circles*) and 0.28 mM (*open circles*) free Mg^{2+}-ions. The data were fit to equation: $L(\rho) = Z(1 - e^{-\rho/\rho 0})^n$, as described in Ref. 41, yielding values of $n = 1.25$ for 5 mM free Mg^{2+}-ions (*solid line*) and $n = 18$ for 0.28 mM free Mg^{2+}-ions (*dashed line*), respectively. Each data point and the corresponding standard deviations were derived from three independent measurements from one or two flow cells.

tion, we followed the spatial and temporal changes in free Mg^{2+}-ion distribution in *Dictyostelium* cells by TIRF microscopy using the Mg^{2+}-sensitive dye KMG-104AM that was previously described as a potent marker for measuring Mg^{2+}-ion concentrations within living cells (40). The series of pictures in Fig. 5*B* show extensive fluctuations of fluorescence in the millisecond to seconds range at tubulovesicular structures that encompass the entire cellular surface (see supplemental Movie 2).

Cellular Localization of Dd Myosin-5b—*Dd* myosin-5b is produced in *Dictyostelium* cells throughout development. Expression levels are high during the first 18 h followed by a marked reduction during later stages of the development cycle (28). We determined the cellular localization of *Dd* myosin-5b during vegetative growth and early development in cells producing full-length protein tagged at the N terminus with YFP by confocal microscopy. The images revealed that *Dd* myosin-5b concentrates at highly dynamic tubular and ring-like structures (Fig. 5*A*). This pattern is characteristic for the contractile vacuole system of the organism (43). The contractile vacuole system in *Dictyostelium* is a dynamic organelle with an osmoregulatory function, collecting fluid in a network of cisternae and tubular structures and releasing it out of the cell through transient, plasma membrane-associated pores (44).

DISCUSSION

Dd myosin-5b is a dimeric motor that consists of two heavy chains, each with a molecular mass of 258 kDa and six associated light chains. *Dd* myosin-5b is assumed to localize at the contractile vacuole (28), a specialized organelle for the regulation of osmotic pressure (44). Recent phylogenetic analyses of more than 1700 myosins from various species places *Dd* myosin-5b and the closely related smaller isoenzyme *Dd* myosin-5a (previously referred to as Myo H) among the class 5 myosins (45, 46). Notable kinetic features of *Dd* myosin-5b emphasizing its close relation to processive class 5 myosins are summarized in Tables 1 and 2 and include slow rates of ADP release (k_{-AD}), ATP binding to actomyosin (K_1k_{+2}), and ATP-induced actin dissociation (k_{+2}). Additionally, ATP hydrolysis is fast ($k_{+3} + k_{-3}$), ADP has only a minor effect on actin binding and dissociation (k_{+DA} and k_{-DA}), and coupling between actin and nucleotide binding (K_{AD}/K_D) is low. The simultaneous occurrence of these kinetic properties is indicative for *Dd* myosin-5b being a high duty ratio motor that populates predominantly the strong actin binding states A·M and A·M·ADP (Scheme 1). The high duty ratio derives primarily from the slow rate of ADP release, which becomes rate-limiting for steady state turnover in the presence of actin. A slow rate of ATP-binding to actomyosin and a fast rate of ATP hydrolysis (>300 s^{-1}) contribute further to a predominant population of strong binding states. However, particular steps in the ATPase cycle of *Dd* myosin-5b do critically depend on the concentration of free Mg^{2+}-ions. We have reported earlier that changes in the physiological concentration of free Mg^{2+}-ions modulate the kinetic properties of *Dd* myosin-1E (38) and *Dd* myosin-1D (47). High free Mg^{2+} concentrations reduce the motile activity of these myosin motors by inhibiting the rate of ADP dissociation from actomyosin. As a consequence, high concentrations of free Mg^{2+}-ions stabilize the tension-bearing acto·myosin·ADP state and shift the actomyosin system from the production of rapid movement toward the generation of tension. In an independent study with vertebrate myosin-5a Sweeney and co-workers (48) reported that free Mg^{2+}-ions have an influence on the rate and order of product release. In accordance to these studies, we

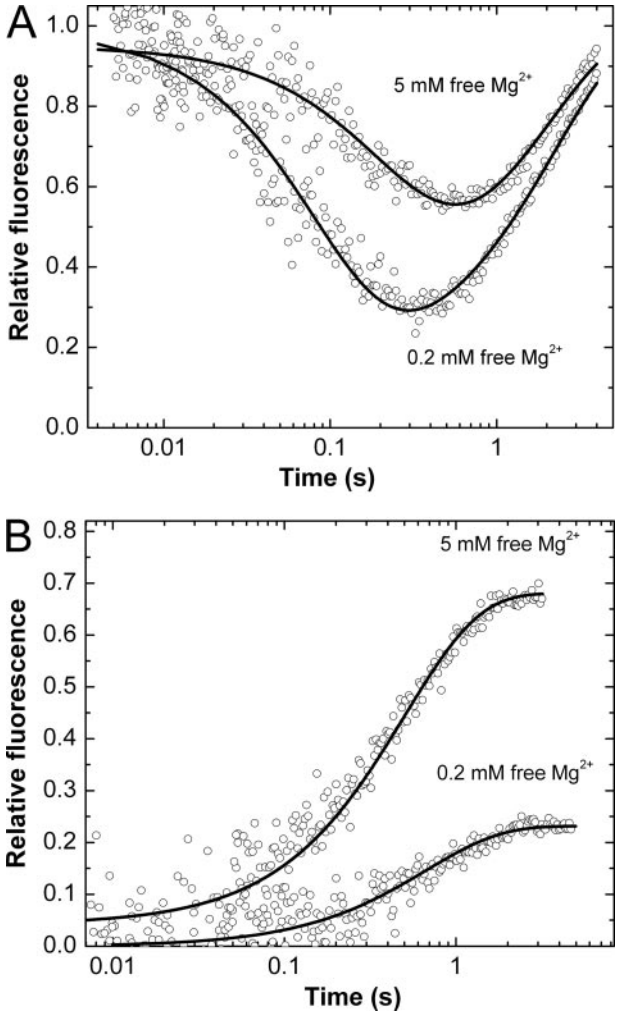

FIGURE 4. **Influence of free Mg^{2+}-ions on the population of the strong actin binding states of *Dd* myosin-5b.** *A*, determination of the dissociation rate constants of the acto·*Dd* myosin-5b complex by excess ATP at different concentrations of free Mg^{2+}. Final concentrations: 1 μM myosin-5b, 7.5 μM pyrene-actin. *B*, determination of the rate constants for the weak-to-strong transition at different free Mg^{2+} concentrations by a sequential mixing experiment. Conditions at time point 0 are: 1 μM *Dd* myosin-5b, 5 μM pyrene-actin, 50 μM ATP, 500 μM ADP. The fluorescence intensities were normalized relative to the maximum fluorescence intensity of 1 that corresponds to 100% of myosin bound to actin.

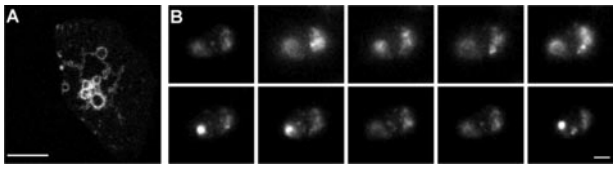

FIGURE 5. **Cellular localization of *Dd* myosin-5b and free Mg^{2+}-ions.** *A*, cellular localization of YFP-tagged *Dd* myosin-5b. The image shows a confocal plane of a *Dictyostelium* Ax2-cell producing YFP-*Dd* myosin-5b. The protein associates with a tubulovesicular network that corresponds to the contractile vacuole system. *Bar*, 10 μm. *B*, tracking of local and temporal changes in free Mg^{2+}-ion distribution in *Dictyostelium* cells by TIRF microscopy. The time series show a *Dictyostelium* cell that was preloaded with the Mg^{2+}-ion-sensitive fluorescent dye KMG-104AM. The time interval between individual images corresponds to 0.5 s and the image sequences proceeds from *top left* to *bottom right corner*. *Bar*, 10 μm.

have observed that high free Mg^{2+}-ion concentrations lead to a reduction in the coupling ratio of actin and ADP binding of *Dd* myosin-5b ($\mathbf{K_{AD}}/K_D \approx 1$). Under these conditions *Dd* myosin-5b is able to bind both F-actin and ADP with high affinity. However, in the presence of low free Mg^{2+}-ion concentrations, $\mathbf{K_{AD}}$ is 5-fold increased (27.9 μM), K_D is almost unaffected, and the coupling ratio ($\mathbf{K_{AD}}/K_D$) is ~5-fold increased. Our *in vitro* motility experiments show that Mg^{2+}-dependent alterations in this order of magnitude directly affect the motile activity of the motor. At ~50 μM free Mg^{2+}-ions *Dd* myosin-5b displays its highest sliding velocity, whereas free Mg^{2+}-ion concentration >1 mM reduce the velocity up to 3-fold. This behavior is due to the reduced ADP release rate from actomyosin, which in turn results in an increased accumulation of the strong binding intermediate state A·M·ADP. From this experiment we conclude that high physiological concentrations of free Mg^{2+} can extend the time the motor spends in strongly bound states up to 3-fold. We investigated this behavior by determining the duty ratio of the motor at low and high free Mg^{2+} concentrations with the aid of the Equation 2, where T_{strong} defines the time the motor spends in the strong actin binding states and T_{total} the overall ATPase cycle time.

$$\text{Duty ratio} = \frac{(1/\mathbf{k_{-AD}}) + (1/\mathbf{k_{+2}})}{(1/k_{cat})} = \frac{T_{strong}}{T_{total}} \qquad \text{(Eq. 2)}$$

Using the parameters $k_{-AD} = 21.6\ s^{-1}$, $k_{+2} = 75\ s^{-1}$, and $k_{cat} = 12.4\ s^{-1}$ that were obtained at 5 mM free Mg^{2+}-ions according to Tables 1 and 2, the calculated duty ratio of *Dd* myosin-5b equals 0.74. This value is in good agreement with the experimentally determined duty ratio of 0.68 that was obtained under the same conditions at 5 μM F-actin concentrations (Fig. 4*B*). Because the duty ratio depends on the actin concentration, it is expected that higher actin concentrations would lead to a further increase of the duty ratio, thus approaching the calculated value of 0.74, which is representative for high actin concentrations. In contrast, at low concentrations of free Mg^{2+}-ions (0.2 mM), the rate of ADP release from acto·*Dd* myosin-5b increases ~10-fold (from 21.6 to 187 s^{-1}), ATP binding becomes 3-fold faster (Fig. 4*A*), and the fraction of strongly bound states decreases more than 3-fold (Fig. 4*B*). The calculated and experimentally determined duty ratio is identical under these conditions (duty ratio = 0.23). The modulation of velocity and duty ratio suggests that *Dd* myosin-5b can switch between working either as a stepping motor or as a motor that is adapted for tension bearing. The results from the landing assays confirm this hypothesis and indicate that *Dd* myosin-5b is a processive motor in the higher physiological range of free Mg^{2+}-ion concentrations and a non-processive in the lower range. We conclude that this kind of conditional adaptation of the mechanoenzymatic mechanism is important in cellular processes that require a cyclical switching between fast contractile activity and slow tension bearing. In agreement with this assumption, our results show that *Dd* myosin-5b localizes at the contractile vacuole (see Fig. 5 and supplemental Movie 1), where it appears to be actively involved in the fast contraction phase and the subsequent phase when expansion of the vacuole volume is suppressed.

The concentration of free Mg^{2+}-ions inside the cell varies in the range from 0.1 to 1 mM (42). The use of a new generation of Mg^{2+}-sensitive fluorescent dyes allows the direct observation

of these changes with greater special and temporal resolution. Here, we have shown that similar changes as observed for HL60, HC11, and PC12 cells (49, 50) do occur in *Dictyostelium* (see Fig. 5*B* and supplemental Movie 2). The observed fluctuations take place in the millisecond range and thus within a time domain where the consequences for myosin motor activity are of physiological relevance.

Acknowledgments—We thank S. Zimmermann, C. Waßmann, and C. Thiel for excellent technical assistance, and N. Tzvetkov for help and discussions. The magnesium fluorescent probe KMG-104AM was kindly provided by Dr. Hirokazu Komatsu and Prof. Koji Suzuki, Keio University, Japan.

REFERENCES

1. Desnos, C., Huet, S., and Darchen, F. (2007) *Biol. Cell* **99,** 411–423
2. Desnos, C., Huet, S., Fanget, I., Chapuis, C., Bottiger, C., Racine, V., Sibarita, J. B., Henry, J. P., and Darchen, F. (2007) *J. Neurosci.* **27,** 10636–10645
3. Boldogh, I. R., Fehrenbacher, K. L., Yang, H. C., and Pon, L. A. (2005) *Gene* (*Amst.*) **354,** 28–36
4. Levi, V., Gelfand, V. I., Serpinskaya, A. S., and Gratton, E. (2006) *Biophys. J.* **90,** L07–L09
5. Evans, L. L., Lee, A. J., Bridgman, P. C., and Mooseker, M. S. (1998) *J. Cell Sci.* **111**, 2055–2066
6. Varadi, A., Tsuboi, T., and Rutter, G. A. (2005) *Mol. Biol. Cell* **16,** 2670–2680
7. Lise, M. F., Wong, T. P., Trinh, A., Hines, R. M., Liu, L., Kang, R., Hines, D. J., Lu, J., Goldenring, J. R., Wang, Y. T., and El-Husseini, A. (2006) *J. Biol. Chem.* **281,** 3669–3678
8. Yoshimura, A., Fujii, R., Watanabe, Y., Okabe, S., Fukui, K., and Takumi, T. (2006) *Curr. Biol.* **16,** 2345–2351
9. Walker, M. L., Burgess, S. A., Sellers, J. R., Wang, F., Hammer, J. A., 3rd, Trinick, J., and Knight, P. J. (2000) *Nature* **405,** 804–807
10. Burgess, S., Walker, M., Wang, F., Sellers, J. R., White, H. D., Knight, P. J., and Trinick, J. (2002) *J. Cell Biol.* **159,** 983–991
11. Coureux, P. D., Sweeney, H. L., and Houdusse, A. (2004) *EMBO J.* **23,** 4527–4537
12. Terrak, M., Rebowski, G., Lu, R. C., Grabarek, Z., and Dominguez, R. (2005) *Proc. Natl. Acad. Sci. U. S. A.* **102,** 12718–12723
13. Trybus, K. M., Gushchin, M. I., Lui, H., Hazelwood, L., Krementsova, E. B., Volkmann, N., and Hanein, D. (2007) *J. Biol. Chem.* **282,** 23316–23325
14. Burgess, S. A., Yu, S., Walker, M. L., Hawkins, R. J., Chalovich, J. M., and Knight, P. J. (2007) *J. Mol. Biol.* **372,** 1165–1178
15. Thirumurugan, K., Sakamoto, T., Hammer, J. A., 3rd, Sellers, J. R., and Knight, P. J. (2006) *Nature* **442,** 212–215
16. Mehta, A. D., Rock, R. S., Rief, M., Spudich, J. A., Mooseker, M. S., and Cheney, R. E. (1999) *Nature* **400,** 590–593
17. Baker, J. E., Krementsova, E. B., Kennedy, G. G., Armstrong, A., Trybus, K. M., and Warshaw, D. M. (2004) *Proc. Natl. Acad. Sci. U. S. A.* **101,** 5542–5546
18. Yildiz, A., Forkey, J. N., McKinney, S. A., Ha, T., Goldman, Y. E., and Selvin, P. R. (2003) *Science* **300,** 2061–2065
19. De La Cruz, E. M., Wells, A. L., Rosenfeld, S. S., Ostap, E. M., and Sweeney, H. L. (1999) *Proc. Natl. Acad. Sci. U. S. A.* **96,** 13726–13731
20. Trybus, K. M., Krementsova, E., and Freyzon, Y. (1999) *J. Biol. Chem.* **274,** 27448–27456
21. Watanabe, S., Mabuchi, K., Ikebe, R., and Ikebe, M. (2006) *Biochemistry* **45,** 2729–2738
22. Watanabe, S., Watanabe, T., Sato, O., Awata, J., Homma, K., Umeki, N., Higuchi, H., Ikebe, R., and Ikebe, M. (2008) *J. Biol. Chem.* **283,** 10581–10592
23. Takagi, Y., Yang, Y., Fujiwara, I., Jacobs, D., Cheney, R. E., Sellers, J. R., and Kovacs, M. (2008) *J. Biol. Chem.* **283,** 8527–8537
24. Toth, J., Kovacs, M., Wang, F., Nyitray, L., and Sellers, J. R. (2005) *J. Biol. Chem.* **280,** 30594–30603
25. Reck-Peterson, S. L., Tyska, M. J., Novick, P. J., and Mooseker, M. S. (2001) *J. Cell Biol.* **153,** 1121–1126
26. Dunn, B. D., Sakamoto, T., Hong, M. S., Sellers, J. R., and Takizawa, P. A. (2007) *J. Cell Biol.* **178,** 1193–1206
27. Peterson, M. D., Urioste, A. S., and Titus, M. A. (1996) *J. Muscle Res. Cell Motil.* **17,** 411–424
28. Hammer, J. A., 3rd, and Jung, G. (1996) *J. Biol. Chem.* **271,** 7120–7127
29. Knetsch, M. L., Tsiavaliaris, G., Zimmermann, S., Ruhl, U., and Manstein, D. J. (2002) *J. Muscle Res. Cell Motil.* **23,** 605–611
30. Anson, M., Geeves, M. A., Kurzawa, S. E., and Manstein, D. J. (1996) *EMBO J.* **15,** 6069–6074
31. Kurzawa, S. E., Manstein, D. J., and Geeves, M. A. (1997) *Biochemistry* **36,** 317–323
32. Egelhoff, T. T., Titus, M. A., Manstein, D. J., Ruppel, K. M., and Spudich, J. A. (1991) *Methods Enzymol.* **196,** 319–334
33. Manstein, D. J., and Hunt, D. M. (1995) *J. Muscle Res. Cell Motil.* **16,** 325–332
34. Lehrer, S. S., and Kerwar, G. (1972) *Biochemistry* **11,** 1211–1217
35. Criddle, A. H., Geeves, M. A., and Jeffries, T. (1985) *Biochem. J.* **232,** 343–349
36. Furch, M., Fujita-Becker, S., Geeves, M. A., Holmes, K. C., and Manstein, D. J. (1999) *J. Mol. Biol.* **290,** 797–809
37. Bagshaw, C. R. (1975) *FEBS Lett.* **58,** 197–201
38. Durrwang, U., Fujita-Becker, S., Erent, M., Kull, F. J., Tsiavaliaris, G., Geeves, M. A., and Manstein, D. J. (2006) *J. Cell Sci.* **119,** 550–558
39. Rock, R. S., Rice, S. E., Wells, A. L., Purcell, T. J., Spudich, J. A., and Sweeney, H. L. (2001) *Proc. Natl. Acad. Sci. U. S. A.* **98,** 13655–13659
40. Komatsu, H., Iwasasa, N., Citterio, D., Suzuki, Y., Kubota, T., Tokuno, K., Kitamura, Y., Oka, K., and Suzuki, K. (2004) *J. Am. Chem. Soc.* **126,** 16353–16360
41. Hancock, W. O., and Howard, J. (1998) *J. Cell Biol.* **140,** 1395–1405
42. Kim, H. M., Yang, P. R., Seo, M. S., Yi, J. S., Hong, J. H., Jeon, S. J., Ko, Y. G., Lee, K. J., and Cho, B. R. (2007) *J. Org. Chem.* **72,** 2088–2096
43. Gabriel, D., Hacker, U., Kohler, J., Muller-Taubenberger, A., Schwartz, J. M., Westphal, M., and Gerisch, G. (1999) *J. Cell Sci.* **112,** 3995–4005
44. Gerisch, G., Heuser, J., and Clarke, M. (2002) *Cell Biol. Int.* **26,** 845–852
45. Foth, B. J., Goedecke, M. C., and Soldati, D. (2006) *Proc. Natl. Acad. Sci. U. S. A.* **103,** 3681–3686
46. Kollmar, M. (2006) *BMC Genomics* **7,** 183
47. Fujita-Becker, S., Durrwang, U., Erent, M., Clark, R. J., Geeves, M. A., and Manstein, D. J. (2005) *J. Biol. Chem.* **280,** 6064–6071
48. Rosenfeld, S. S., Houdusse, A., and Sweeney, H. L. (2005) *J. Biol. Chem.* **280,** 6072–6079
49. Suzuki, Y., Komatsu, H., Ikeda, T., Saito, N., Araki, S., Citterio, D., Hisamoto, D., Kitamura, Y., Kubota, T., Nakagawa, J., Oka, K., and Suzuki, K. (2002) *Anal. Chem.* **74,** 1423–1428
50. Farrugia, G., Lotti, S., Prodi, L., Montalti, M., Zaccherroni, N., Savage, P. B., Trapani, V., Sale, P., and Wolf, F. I. (2006) *J. Am. Chem. Soc.* **128,** 344–350